ELSEVIER

Journal of Nuclear Materials 298 (2001) 95–111

journal of nuclear materials

www.elsevier.com/locate/jnucmat

Near-field performance assessment for a low-activity waste glass disposal system: laboratory testing to modeling results

B.P. McGrail [a,*], D.H. Bacon [a], J.P. Icenhower [a], F.M. Mann [b], R.J. Puigh [c], H.T. Schaef [a], S.V. Mattigod [a]

[a] *Applied Geology and Geochemistry Department, Pacific Northwest National Laboratory, 902 Battelle Boulevard, P.O. Box 999, MS K6-81, Richland, WA 99352, USA*

[b] *CH2M Hill Inc., Richland, WA 99352, USA*

[c] *Fluor Federal Services, Richland, WA 99352, USA*

Abstract

Reactive chemical transport simulations of glass corrosion and radionuclide release from a low-activity waste (LAW) disposal system were conducted out to times in excess of 20 000 yr with the subsurface transport over reactive multiphases (STORM) code. Time and spatial dependence of glass corrosion rate, secondary phase formation, pH, and radionuclide concentration were evaluated. The results show low release rates overall for the LAW glasses such that performance objectives for the site will be met by a factor of 20 or more. Parameterization of the computer model was accomplished by combining direct laboratory measurements, literature data (principally thermodynamic data), and parameter estimation methods.

PACS: 28.41.Kw; 47.70.Fw; 81.05.Kf

1. Introduction

The Hanford Site in southeastern Washington State has been used extensively to produce nuclear materials for the US strategic defense arsenal by the US Department of Energy (DOE). A large inventory of radioactive and mixed waste has accumulated in 177 buried single- and double-shell tanks. Liquid waste recovered from the tanks will be pretreated to separate the low-activity fraction from the high-level and transuranic wastes. The low-activity waste (LAW) will be immobilized in glass and placed in a near-surface disposal system on the Hanford Site. Vitrifying the LAW will generate over 160 000 m^3 of glass. The immobilized low-activity waste (ILAW) at Hanford is among the largest volumes of waste within the DOE complex and is one of the largest inventories of long-lived radionuclides planned for disposal in a low-level waste facility (approximately 2.4 million curies total activity). Before the ILAW can be disposed, DOE must approve a performance assessment (PA), which is a document that describes the long-term impacts of the disposal facility on public health and environmental resources. A sound scientific basis for determining the long-term release rates of radionuclides from LAW glasses must be developed if the PA is to be accepted by regulatory agencies, stakeholders, Native Americans, and the public.

The technical strategy being employed to conduct the Hanford ILAW PA [1] is similar to the methodology being used to analyze the Drigg low-level waste site in the UK [2], where the modeling is fundamentally deterministic and based on a coupled flow and reactive chemical transport simulation of the near field environment. Deterministic PAs but with much simpler models describing radionuclide release and transport are being used for high-level waste repositories in Sweden [3] and in Japan [4]. In contrast, probabilistic approaches are being used for the US high-level waste repository [5] and for the transuranic waste site at the Waste Isolation Pilot Plant [6]. For the Hanford ILAW PA [7], the deterministic approach is preferred to avoid the use of

* Corresponding author. Tel.: +1-509 376 9193; fax: +1-509 376 2210.

E-mail address: pete.mcgrail@pnl.gov (B.P. McGrail).

0022-3115/01/$ - see front matter
PII: S0022-3115(01)00576-1

'abstraction,' which simplifies radionuclide release models into forms that can be executed tens of thousands of times in a probabilistic simulator [8]. The deterministic approach allows direct implementation of chemical rate laws governing radionuclide release and transport into the simulator so that impacts of important coupled processes can be rigorously evaluated. Also, direct implementation of chemical rate laws avoids use of empirical 'leach rates' derived from laboratory experiments that are commonly used in other performance assessments. Such extrapolations are not technically defensible for Hanford ILAW because:

1. The dissolution rate, and hence radionuclide release rate from silicate glasses is not a state function, i.e. a constant that can be derived independent of other variables in the system. Glass dissolution rate is a function of three variables (neglecting glass composition itself): temperature, pH, and composition of the fluid contacting the glass. The temperature of the ILAW disposal system is a known constant. However, both pH and composition of the fluid contacting the glass are variables that are affected by flow rate, reactions with other engineered materials, gas-water equilibria, secondary phase precipitation, alkali ion exchange, and by dissolution of the glass itself (a classic feedback mechanism). Consequently, glass dissolution rates will vary both in time and as a function of position in the disposal system. There is no physical constant such as a 'leach rate' or radionuclide release rate parameter that can be assigned to a glass waste form in such a dynamic system.
2. One of the principal purposes of the ILAW PA is to provide feedback to engineers regarding the impacts of design options on disposal system performance. A model based on empirical release behavior of the waste form could not provide this information. For example, we have found little effect on waste form performance regardless of whether stainless or cast steel is used for the waste form pour canister. However, significant impacts have been observed when large amounts of concrete are used in constructing vaults for ILAW. The concrete raises the pH of the pore water entering the waste packages and so increases glass corrosion.

In this paper, we will describe the methodology employed to obtain the necessary input data to conduct computer simulations of glass corrosion and radionuclide transport from a LAW disposal system. Experiments were used to examine glass corrosion behavior, to provide the required data to parameterize a kinetic rate law for glass dissolution, and to calibrate a reaction network for conducting reactive transport simulations of the disposal system. First, an overview of the ILAW disposal system is provided followed by a description of the reactive transport computer model used to conduct the PA calculations. In Section 4, the laboratory methods and their use in deriving the necessary input parameters for conducting PA calculations are discussed. Finally, results from PA calculations for a representative LAW glass formulation are discussed followed by conclusions and recommendations.

2. Conceptual disposal facility design for Hanford ILAW

A remote handled (RH) trench concept has been chosen as the baseline for the ILAW Disposal Project. Fig. 1 shows the design concept layout for the waste package loading into the RH trench. A cell is defined as a contiguous group of waste packages in a given layer. A waste package consists of 1.4 m cubic stainless steel (304 L) container, which is 85% filled with LAW glass. The closure cap (surface barrier) is assumed to have the same relative thickness, materials, and slope as the modified RCRA subtitle C closure cap defined by Puigh [9]. Below the closure cap is a capillary break consisting of a 1 m thick sand layer immediately below the surface barrier, followed by a gravel layer between the top of the trench and the sand layer. The function of the capillary break is to divert moisture penetrating the closure cap around the waste packages. The sand plus gravel layers together are 4 m over the center of the trench and have a 2% slope towards the long edge of each trench. The RCRA subtitle C closure cap and the capillary break

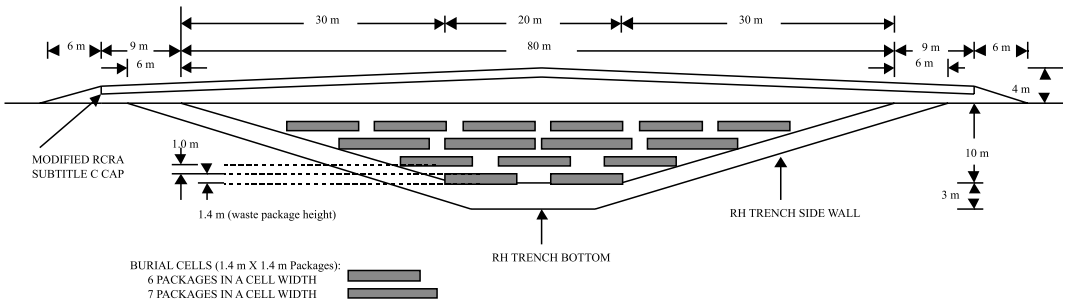

Fig. 1. Remote handled trench pre-conceptual design.

have a combined thickness of greater than 5 m per NRC requirements (10 CFR 61). Six trenches of approximately 260 m in length are required to accommodate a total of over 68 000 individual waste packages.

3. Modeling overview

Past Hanford Site PAs [10,11] have shown the groundwater pathway to be the most restrictive for the vast majority of radionuclides. The eight steps considered for the groundwater pathway are:

1. Precipitation (rain or snow) falls on the ground with much of the water returned to the atmosphere due to evaporation or transpiration through plant leaves. The remaining water infiltrates the soil below the surface at a very low rate.
2. The water moves downward, but some of the water is diverted by an intact sand-gravel capillary break.
3. The water that is not diverted away from the waste may be chemically modified by the local environment, interacts with the waste form, and accumulates contaminants.
4. The water (possibly a reduced amount because waste form dissolution and mineral formation consumes water) leaves the disposal facility carrying contaminants with it. Some contaminants may interact with the material in the disposal facility, slowing the release of contaminants to the surrounding natural environment.
5. Contaminated water moves through the undisturbed, unsaturated zone (vadose zone) below the disposal facility down to the unconfined aquifer. The contaminants may interact with soil sediments causing further retardation. Changes to the properties of the natural system are considered, but are not a major impact on the analysis results.
6. The water and contaminants move and mix with the water in the unconfined aquifer until they are extracted from the aquifer and brought to the surface or until they reach the Columbia River.
7. Contaminants are extracted by being carried to the surface with groundwater being pumped from a well.
8. The contaminants result in human exposure through a variety of exposure pathways (ingestion, inhalation, dermal contact, and external radiation) and exposure scenarios (agricultural, Native American, etc.).

The Hanford ILAW PA consists of the application of computer codes for four purposes:

- to calculate contaminant release rates from the waste packages and from the disposal facility,
- to calculate moisture flow and contaminant transport in the vadose zone,
- to calculate moisture flow and contaminant transport in groundwater, and
- to merge the results of the preceding codes.

Fig. 2 illustrates the overall computational strategy. The focus of this paper is the near-field environment, which is defined as the domain including the trench and a short distance below the floor of the disposal facility. A coupled unsaturated flow, chemical reactions, and contaminant transport simulator (subsurface transport over reactive multiphases (STORM)) is used within the near field [12]. The plume exiting the region near the vault is expected to be of high ionic strength and pH, and will migrate down into the vadose zone. However, at some distance from the disposal vaults, geochemical conditions will approach those more typical of the Hanford vadose zone and for which simplifying assumptions (such as linear sorption, negligible precipitation/dissolution, no changes in hydraulic properties, and no fluid density gradient effects) can be used. This region is defined as the far-field environment and can be simulated using standard, nonreactive (chemical reactions not specifically included in calculations) flow and transport codes. For the ILAW PA, computations in the far-field domain were done using VAM3DF [13], a variably saturated flow and transport code.

The underlying mathematics in STORM is contained in a set of coupled, non-linear, partial differential equations representing conservation equations for energy, mass, and momentum. They describe the rate of change of the solute concentrations of pore water in a variably saturated, nonisothermal porous medium, and the alteration of waste forms, packaging materials,

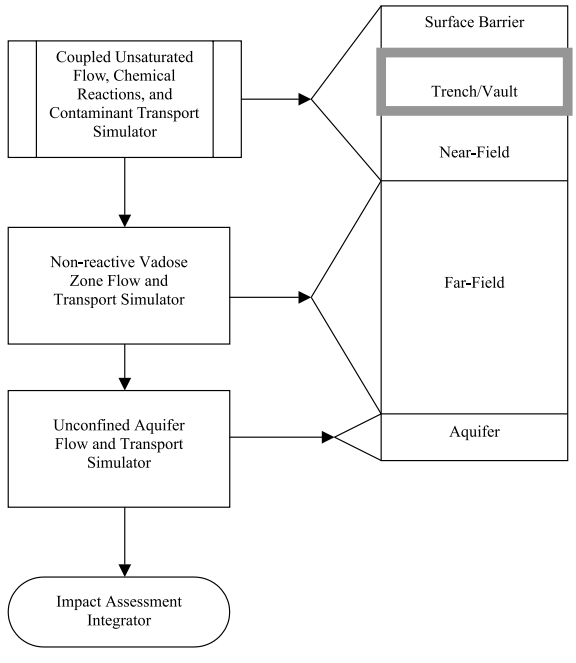

Fig. 2. Modeling strategy for assessing ILAW disposal system.

backfill, and host rocks. The simulator can consider the following topics:

- kinetic dissolution of waste forms,
- kinetic dissolution of host rocks,
- kinetic precipitation and dissolution of secondary phases,
- aqueous equilibrium speciation,
- gas-aqueous equilibria,
- redox reactions,
- two-phase flow (water and air),
- dynamic hydraulic properties.

Other physical and chemical features of the code are:

- 1-D (vertical Z-axis) or 2-D (X–Z Plane) solution domains,
- general interface to take user specified chemistry and hydraulic properties,
- non-isothermal multiphase flow and chemistry,
- ionic strength correction according to modified B-dot equation,
- spatially varying distribution of minerals in solid phase,
- effective reaction surface varies with dissolution and precipitation of solids.

The primary output of STORM, as a function of time and space, consists of the following:

- concentrations of aqueous species,
- concentrations of gaseous species,
- release flux of aqueous species and chemical components,
- pH and Eh changes,
- radii, surface areas, and volume fractions of solids,
- dissolution/precipitation rates of solids,
- production/consumption rates of aqueous species, including water,
- temperature,
- porosity and permeability changes,
- aqueous phase saturations, velocities,
- gas phase saturations, velocities.

The interested reader should consult Bacon et al. [12] for a detailed discussion of the mathematical underpinnings of the STORM code. For the purposes of this paper, the key advantage of using a reactive transport code such as STORM is that the following well-known kinetic rate law for glass dissolution [14,15] can be implemented directly in the simulator:

$$k = \vec{k} a_{\mathrm{H}^+}^{-\eta} \exp\left(\frac{-E_\mathrm{a}}{RT}\right)\left[1 - \left(\frac{Q}{K_\mathrm{g}}\right)^{\sigma}\right]\prod_j a_j^{\eta_j}, \qquad (1)$$

where k is the dissolution rate (g m^{-2} d^{-1}); $\vec{k}$ the intrinsic rate constant (g m^{-2} d^{-1}); a_{H^+} the hydrogen ion activity; a_j the activity of the jth aqueous species that acts as an inhibitor or as a catalyst of dissolution; E_a the activation energy (kJ mol^{-1}); R the gas constant (kJ mol^{-1} K^{-1}); T the temperature (K); Q the ion activity product; K_g the pseudoequilibrium constant for glass; η the power law coefficient; σ is the Temkin coefficient.

Assuming that $\vec{k}$, E_a, η, K_g, and σ are all known parameters developed from laboratory testing, and the disposal system temperature is a constant 15°C, calculation of the glass dissolution rate via Eq. (1) simply requires calculation of the pH and ion activity product, Q, neglecting the $\prod a_j^{\eta_j}$ term. This calculation is repeated at each grid node for each time step to build-up a time and spatially dependent picture of glass dissolution rate in the disposal system.

The reader should note that we have implicitly assumed that kinetic rate law (1) correctly describes the effect of solution composition on the glass dissolution rate. However, there is considerable disagreement about this assumption in the literature. Strachan et al. [16] conclude that of all the models that have been developed to describe glass dissolution behavior, the kinetic rate law (1) best describes the majority of the experimental data that has been gathered over 35 years of studying glass/water reaction processes. Consequently, we have elected to use this rate equation for modeling glass dissolution behavior in the ILAW disposal system. However, French investigators [17,18] have recently argued that 'protective layers,' a popular theory in the early 1980s, better describe experimental results for SON 68 high-level waste glass. The principal difficulty with 'passivating layer' models is that the current models are totally empirical. The protective nature of the layer appears to depend on as yet unquantified parameters and on the conditions under which it formed. It also appears that the protective properties of the alteration layers must be time dependent. McGrail et al. [19] show a very rapid transition (hours) from a low rate of glass corrosion to a rate near the forward rate of reaction in pressurized unsaturated flow (PUF) experiments with a LAW glass, which was correlated with the onset of zeolite precipitation. It would appear to be very difficult to develop a mass transport barrier model where the properties of the passivating layer could change so dramatically so rapidly. Without a specific mathematical formulation for the protective layer model, and because of the still considerable doubt about the validity of the hypothesis itself, we select the chemical affinity-based rate law for use in modeling the ILAW disposal system.

Having described the general approach for near-field modeling, a description of the methods used to parameterize the STORM model is discussed in the following section.

4. Experimental methods

4.1. Materials

The experiments and PA calculations described in this paper were performed for a representative LAW glass called LAWABP1. The composition of this glass is

Table 1
Composition stoichiometry (υ_i) of LAWABP1 glass

Element	υ_i	Element	Mol fraction
Al	1.36×10^{-1}	O	1.87×10^{-0}
B	1.84×10^{-1}	P	7.79×10^{-4}
Cl	1.13×10^{-2}	Pu	3.52×10^{-8}
Cr	1.82×10^{-4}	^{99}Tc	6.59×10^{-7}
F	1.46×10^{-3}	S	8.63×10^{-4}
Fe	2.16×10^{-2}	^{79}Se	1.77×10^{-8}
^{129}I	1.54×10^{-7}	Si	4.82×10^{-1}
K	3.23×10^{-2}	Ti	2.15×10^{-2}
La	8.48×10^{-3}	U	9.81×10^{-5}
Mg	1.71×10^{-2}	Zn	2.20×10^{-2}
Na	4.46×10^{-1}	Zr	2.94×10^{-2}

given in Table 1. This glass was selected because it was observed to have superior durability as compared with other LAW glasses tested in our laboratory, principally via PUF [20] and vapor hydration test (VHT) methods [21].

4.2. Kinetic rate law parameters for glass

Although Eq. (1) has been used extensively to model glass dissolution kinetics, there is still considerable debate in the scientific community regarding the parameterization of this equation. For example, it is well established that dissolution rates increase with an increase in the activity of the hydroxyl ion (i.e., pH), but it is not clear if other aqueous species inhibit or catalyze reaction rates. It is generally recognized, for example, that aluminum in solution causes a decrease in reaction rates of aluminosilicate materials [22], yet there is disagreement over how this effect should be taken into account in Eq. (1). For example, some investigators advocate that the activity of aluminate and even silicic acid should be represented as an inhibitor term [23] like the hydrogen ion activity. Other investigators have proposed that the aluminate activity should be part of the pseudoequilibrium constant, along with the activity of silicic acid [24]. An additional uncertainty rests with the nature and value of the Temkin coefficient, σ, which represents the net reaction order. Investigators have reported values of σ ranging between 0.4 and 1 whereas others have recommended that σ should be ignored in the above equation because any value where $\sigma \neq 1$ is inconsistent with transition state theory [25]. We have assumed $\sigma = 1$ for this work.

The single-pass flow-through (SPFT) method was used to determine $\vec{k}, E_a, \eta$, and K_g in Eq. (1). The SPFT test is an open system test where a solution at a known flow rate and constant temperature flows through a reaction cell that contains the sample. The configuration precludes recirculation of a portion of the effluent and so makes a 'single-pass' through the reaction cell. Many different SPFT apparatuses have been developed, but these can all be classified as three basic types: (1) well-mixed batch, (2) packed bed, and (3) fluidized bed. The well-mixed batch type of apparatus was used for all test data reported here.

Only a brief description of the SPFT method is provided. The interested reader should refer to McGrail et al. [26] for a detailed description of the experimental method. SPFT experiments utilize Teflon reactor vessels that are connected to Teflon tubing that transport aqueous solutions from the input reservoir through tubing that carries solution to the collection vials. Computerized syringe or infusion pumps precisely control flow of aqueous solutions into the reactors. Reactors are housed in constant temperature ovens and powdered samples (typically the 75–150 μm size fraction) react with the volume of solution within the vessel. Effluent samples are collected continuously and aliquots are periodically retained for analysis. Concentrations of the elements are determined by precision inductively coupled plasma optical emission (ICP-OES) and mass spectrometry (ICP-MS) methods. Input solutions are made by combining deionized water, tris hydroxymethyl aminomethane (THAM), and nitric acid in variable amounts to yield solutions buffered at pH values of 2–10. Variable amounts of LiOH, stabilized by LiCl, make up solutions with pH values to 11. The effect of variable silicon (up to saturation with respect to amorphous silica) and aluminum (up to 500 ppb Al) were used to explore the effects of solution composition on reaction rates. All input solutions are continuously sparged by nitrogen gas to prevent deviations from the initial pH values.

Apparent dissolution rates are calculated from the expression

$$\text{rate}_i = \frac{(C_i^{\text{out}} - C_i^{\text{in}})q}{f_i S}, \tag{2}$$

where rate_i is the apparent dissolution rate of the glass sample as indexed by element i (g m^{-2} d^{-1}); C_i^{out} the concentration of the element of interest in the effluent (g l^{-1}); C_i^{in} the concentration of the element of interest in the feed solution (g l^{-1}); q the solution flow-through rate (l d^{-1}); f_i the mass fraction of the element in the glass (dimensionless); S is the surface area of the material (m^2).

Blanks (effluent samples run through the system without glass powders) establish background concentrations of elements of interest in the input solution. The SPFT experiments were conducted for periods of up to 56 days or until steady-state effluent concentrations were obtained.

4.2.1. Estimation of $\vec{k}, E_a, \eta$

Fig. 3 shows the forward dissolution rate data for LAWABP1 glass as a function of pH and temperature.

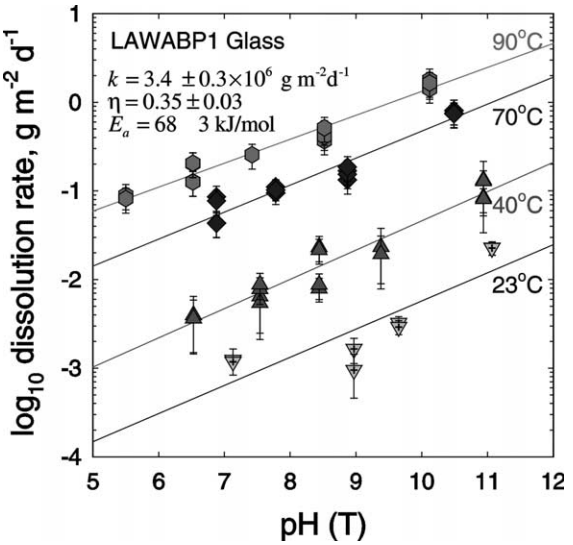

Fig. 3. Plot of forward reaction rate as a function of pH and temperature for LAWABP1 glass.

Because the solutions were kept dilute during the SPFT experiments, the chemical affinity term $(1 - Q/K)$ in Eq. (1) can be neglected and a nonlinear regression performed to estimate the three unknown terms $(\bar{k}, E_a, \eta)$. The results of the regression give $\bar{k} = 3.4 \pm 0.3 \times 10^6\,\mathrm{g\,m^{-2}\,d^{-1}}$, $\eta = 0.35 \pm 0.03$, and $E_a = 68 \pm 3\,\mathrm{kJ\,mol^{-1}}$. The pH dependence of the forward reaction rate is consistent with our previous measurements for LD6-5412 glass [26], where $\eta = 0.40 \pm 0.03$. The 68 kJ mol^{-1} activation energy for LAWABP1 glass is somewhat lower than the 75 kJ mol^{-1} determined for LD6-5412 glass [26].

4.2.2. Estimation of K_g

SPFT experiments have often been used to estimate forward reaction rate constants, activation energies, etc. However, McGrail et al. [26] were the first to use SPFT experiments to derive estimates for the pseudoequilibrium constant, K_g. These results are now extended by performing a series of experiments in which the input concentration of silicic acid was varied from detection limit to near saturation with respect to amorphous silica. Fig. 4 illustrates the observed change in dissolution rate as the Si concentration is increased. This data set clearly follows a non-linear relationship, which is not consistent with the linear rate law proposed by Grambow [15].

A number of investigators have showed that dissolution rates are not linearly dependent on Si concentrations. These investigators proposed that glass dissolution is governed by the activities of aluminum and silicon in solution [24,27,28]. Gin [24] advocates a mixed Al–Si activity product formulation

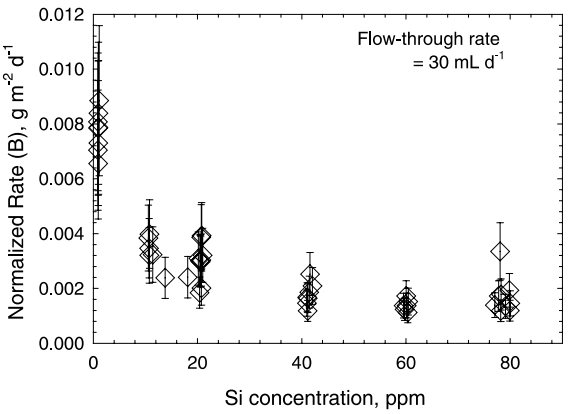

Fig. 4. Plot of dissolution rate (boron) versus silicon concentration for LAWABP1 glass at 40°C and pH (25°C) = 9.

$$K_g = a[\mathrm{AlO_2^-}]^{\upsilon_{Al}} \cdot a[\mathrm{SiO_2(aq)}]^{\upsilon_{Si}}, \tag{3}$$

where a denotes the activities of the species $\mathrm{AlO_2^-}$ and $\mathrm{SiO_2(aq)}$, and υ_{Al} and υ_{Si} represent the stoichiometric coefficient of aluminum and silicon in the glass, respectively. In Fig. 5, we plot the dissolution rate of LAWABP1 glass at 40°C as a function of the mixed Al–Si activity product. In these tests, the input solution was doped with both Al and Si at various concentration levels. The data show an excellent linear correlation ($R^2 = 0.92$) and from the x-intercept we find $K_g = 0.008 \pm 0.001$. Consequently, we conclude that a simple mixed Al–Si activity product term best explains the entire set of data for LAWABP1 glass. However, use of this mixed Al–Si activity product formulation in PA calculations can lead to some troubling results, which we will discuss later.

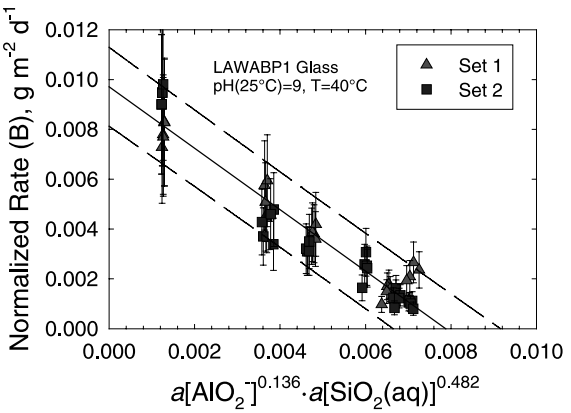

Fig. 5. Normalized release rate as a function of a mixed Al–Si activity product for LAWABP1 glass. Solid line is the best fit from linear regression analysis and the dashed lines are the 95% confidence interval.

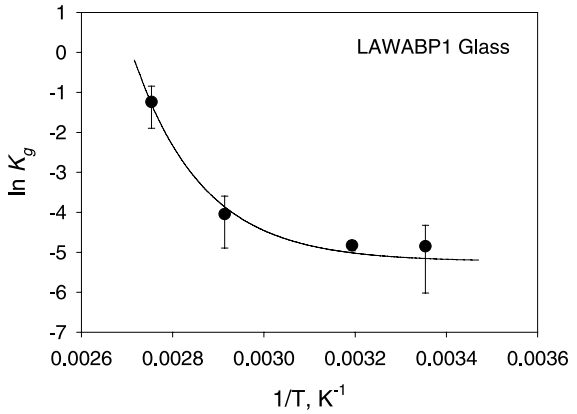

Fig. 6. Temperature dependence of psuedoequilibrium constant for LAWABP1 glass.

Similar experiments were performed at 23°C, 70°C and 90°C so that an extrapolation to the disposal system temperature of 15°C could be made. Although not shown in this paper, the correlation between the mixed Al–Si activity product and dissolution rate was not nearly as good at 90°C and 23°C. The data are also non-linear on an Arrhenius plot (Fig. 6). Consequently, we elected to extrapolate these results to 15°C using an empirical exponential decay function to obtain an estimated $\log K_g(15°C) = -2.2$. This value was then used in several PA simulations with the STORM code.

4.2.3. Sodium ion exchange

LAW glasses contain significant amounts of alkali with desired Na_2O contents of 20 mass% or higher. It was observed in static experiments with several LAW glasses that normalized Na release rates exceeded those of any other element in the glass, including boron [29]. We have attributed this observation to a secondary reaction process, alkali ion exchange. In fact, alkali ion exchange can be the dominant reaction mechanism under certain conditions, such as when the solution in contact with the glass is very near saturation with respect to amorphous silica or at low temperatures, such as those expected for a LAW disposal system. The ion exchange reaction is a true 'leaching' mechanism involving the selective extraction of alkali elements from the glasses. The reader should consult McGrail et al. [30] for more detailed information on alkali ion exchange and how glass structure impacts exchange rates. The importance of this reaction is that it increases the pH of the water in contact with the glass, which can significantly increase release rates (100× or more) when compared with simulations where the ion exchange reaction is excluded [31]. For our purposes in this paper, we simply need a means to measure the exchange rate for LAWABP1 glass so that this reaction can be included in the reaction network for the STORM code.

A convenient means of measuring Na ion-exchange rates is also via SPFT experiments. Experiments conducted in silica-saturated solutions suppress the rate of glass matrix dissolution but have no impact on alkali ion exchange rates because the exchange process is controlled by an independent reaction mechanism. Fig. 7 shows the Na ion-exchange rate as a function of temperature and SiO_2(aq) concentration in the buffer solution. The exchange rate was calculated by subtracting the Na contributed from matrix hydrolysis, as indexed by the rate of boron release, from the total Na release rate. The results show (Fig. 7) that in solutions with no added Si, the Na ion exchange rate cannot be distinguished from a zero rate within experimental error. This is because the glass dissolution dominates over Na ion exchange over the temperature range studied (40–90°C) at low silica concentrations. However, as the input Si concentration is increased, the matrix dissolution rate slows and the differential rate of Na release approaches a constant value indicative of the Na ion-exchange rate. Sodium exchange rates were obtained at each temperature by fitting the data to a simple empirical function of the form $y = a * x/(b + x)$, where a is the Na ion exchange rate at large Si concentrations. The temperature dependent Na exchange rates were then plotted on an Arrhenius diagram to obtain an extrapolated exchange rate at 15°C of 3.4×10^{-11} mol m^{-2} s^{-1} [20]. The exchange reaction is modeled in the STORM code using

$$\text{Glass}\cdots\text{Na} + \text{H}^+ \rightarrow \text{Glass}\cdots\text{H} + \text{Na}^+. \quad (4)$$

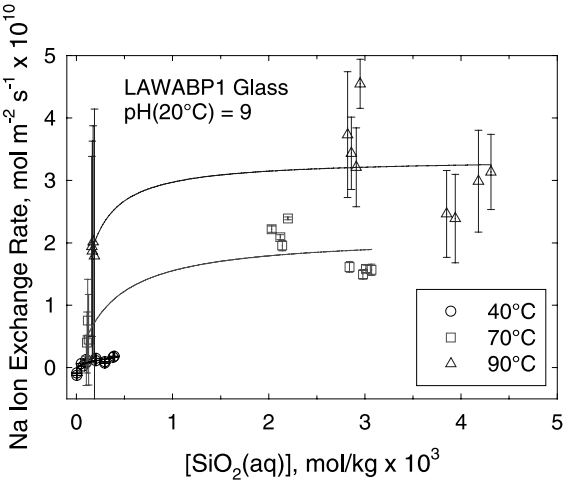

Fig. 7. Excess Na exchange rate from LAWABP1 glass as a function of temperature and SiO_2(aq) concentration. Lines shown are non-linear regression fits using the function $y = a * x/(b + x)$ where a and b are the fitting parameters.

STORM keeps track of the amount of hydrated glass formed via reaction (4) and allows it to dissolve following the identical rate law used for the parent glass.

4.3. Reaction network

Like any geochemically based simulator, calculations with the STORM code require construction of a chemical reaction network consisting of gas–water, aqueous speciation, and dissolution precipitation reactions that are to be considered. The dissolution reaction for LAWABP1 glass is

$$\begin{aligned}
&\text{LAWABP1} + 4.42\times10^{-1}\,H^+ + 1.89\times10^{-1}\,H_2O\\
&\quad\rightarrow 1.36\times10^{-1}\,AlO_2^- + 1.84\times10^{-1}\,B(OH)_3(aq)\\
&\qquad + 1.13\times10^{-2}\,Cl^- + 1.82\times10^{-4}\,CrO_4^{2-}\\
&\qquad + 1.46\times10^{-3}\,F^- + 2.16\times10^{-2}\,Fe(OH)_3(aq)\\
&\qquad + 1.54\times10^{-7}\,IO_3^- + 3.23\times10^{-2}\,K^+\\
&\qquad + 8.48\times10^{-3}\,La^{3+} + 1.71\times10^{-2}\,Mg^{2+}\\
&\qquad + 4.46\times10^{-1}\,Na^+ + 7.79\times10^{-4}\,HPO_4^{2-}\\
&\qquad + 3.52\times10^{-8}\,PuO_2(CO_3)_3^{4-} + 8.63\\
&\qquad \times10^{-4}\,SO_4^{2-} + 1.77\times10^{-8}\,SeO_4^{2-} + 4.82\\
&\qquad \times10^{-1}\,SiO_2(aq) + 6.59\times10^{-7}\,TcO_4^- + 2.15\\
&\qquad \times10^{-2}\,Ti(OH)_4(aq) + 9.81\\
&\qquad \times10^{-7}\,UO_2(OH)_2(aq) + 2.20\times10^{-2}\,Zn^{2+}\\
&\qquad + 2.94\times10^{-2}\,Zr(OH)_4(aq). \qquad (5)
\end{aligned}$$

Previous PAs for ILAW at Hanford [11] have shown that ^{99}Tc is the principal radionuclide of concern because of its high solubility and mobility as the pertechnetate anion (TcO_4^-). Other radionuclides of concern, such as ^{79}Se and ^{129}I, were also considered. However, because these elements are also highly soluble and mobile like Tc, their release rates are directly proportional to that of Tc (scaled by their inventory in the glass) and so were calculated directly from the Tc release rate.

The bulk of the reaction network was developed by simulating PCT [32] experiments with the EQ3/6 code [33]. These simulations were not intended to be representative of disposal system conditions but to make use of the EQ3/6 software to extract a relevant subset of aqueous speciation and mineral precipitation reactions from the large thermodynamic database [34]. Fig. 8 shows a comparison of the EQ3/6 simulations with results from PCT experiments with LAWABP1 glass. The agreement with the experimental data is extraordinarily good. The predicted secondary phase paragenesis is provided in Fig. 9. However, it was necessary to adjust the log K upward for several of the phases [labeled as amorphous, e.g. $La(OH)_3$(am)] to match the observed solution concentration values. This is a consequence of the fact that amorphous solids rather than their crystalline analogs often form in laboratory experiments with waste glasses. The amorphous solids are typically much more soluble and this is reflected in the equilibrium constant. The reaction network was further constrained by eliminating a number of solid phases from consideration because: (1) formation of the phase is kinetically prohibited at the disposal system temperature of 15°C, (2) selection of the phase would violate the Gibbs phase rule, (3) allowing the phase to form caused large deviations from the PCT experimental data, or (4) the phase is unstable over the range of chemical environments expected for the ILAW disposal system.

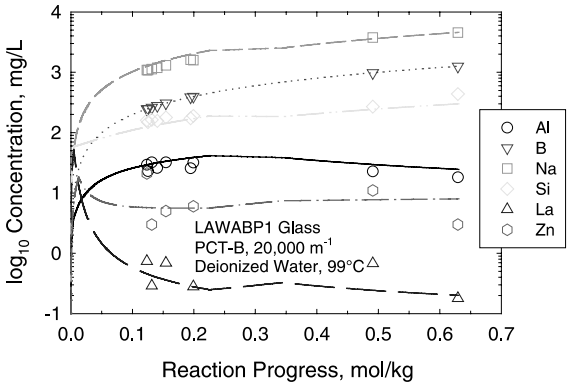

Fig. 8. Comparison of PCT solution concentration data with the solution composition calculated with the EQ3/6 code.

Herschelite [$Na_{1.62}\,K_{0.50}\,Al_{2.26}\,Si_{4.00}\,O_{12.45}\cdot 6H_2O$] was also identified as a ubiquitous reaction product in PUF tests [20] with LAWABP1 glass. Because this phase is thought to be principally responsible for dissolution rate accelerations observed during testing, inclusion of this phase in the reaction network is mandatory. However, a solubility product for this phase is not included in the current thermodynamic database for EQ3/6 nor has a measured value been reported. Consequently, it was necessary to estimate a $\log K$ for herschelite. A ΔG_f^0 value for herschelite was estimated by the method of Mattigod and McGrail [35]. The temperature dependence of the log K for herschelite was then calculated using the heat capacity estimation approach outlined by Mattigod and Kittrick [36]. The dissolution/precipitation reaction of herschelite is expressed in the form

$$\begin{aligned}
&Na_{1.62}K_{0.50}Al_{2.26}Si_{4.00}O_{12.45}\cdot 6H_2O + 8.9H^+\\
&\quad = 1.62Na^+ + 0.50K^+ + 2.26Al^{3+} + 4H_4SiO_4\\
&\qquad + 2.45H_2O \qquad (6)
\end{aligned}$$

and the final function for computing the solubility product of herschelite is

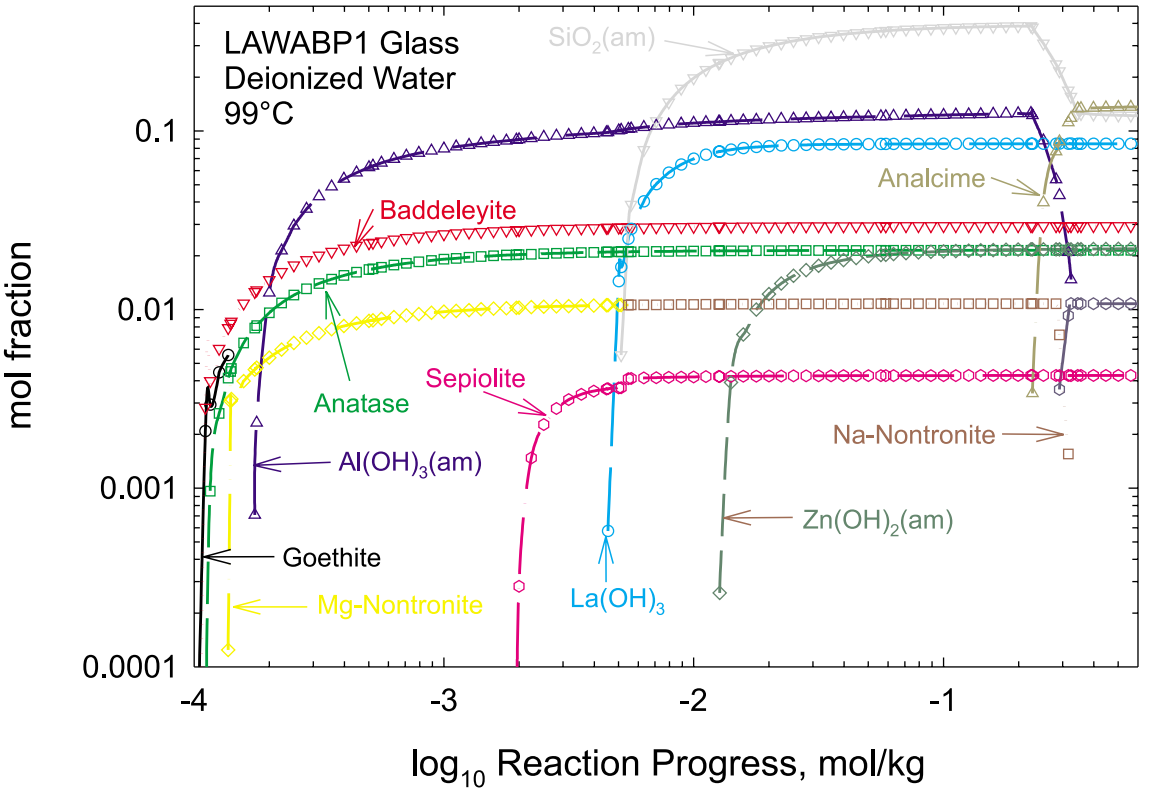

Fig. 9. Predicted paragenetic sequence of alteration phases formed during the reaction of LAWABP1 glass in deionized water. PuO_2 and soddyite were also predicted to form. However, they are not shown because of the very small mol fractions associated with these phases.

$$\log K(T) = -11.5438 \ln T + 0.071779T + 8.8225 \times 10^4/T^2 + 1.1881 \times 10^4/T + 15.654. \quad (7)$$

Additional details on the derivation of Eq. (7) can be found in reference [20]. The final secondary phase reaction network and the associated $\log K$ values used in STORM simulations are provided in Table 2.

5. Modeling

5.1. Setup and parameterization

The majority of the simulations were done using a 1-D vertical profile near the center of a single trench because of long execution times (approximately 1 week on a Sun Ultra workstation) required to achieve simulation times of 20 000 yr. However, results from one two-dimensional simulation using the trench design shown in Fig. 1 will also be presented. For the 1-D simulations, a series of material zones was established as illustrated in Fig. 10. It was assumed that the material representing the waste packages is 85% glass, 2% stainless steel, and 13% backfill (Hanford sand) by volume. The glass was assumed to be sparsely fractured from thermal stresses produced during cooling such that the initial glass surface area was 10X greater than the geometric surface area [37,38]. The backfill material was assumed to consist of 40% albite, 40% quartz, 10% K-feldspar and 10% illite. The waste package containers were assumed to be 304L stainless steel. The corrosion reaction for 304L stainless steel is given by

$$\begin{aligned}\text{Steel} &+ 2.9262 \times 10^{-2}\ H^+ + 1.7618\ H_2O \\ &+ 3.4169 \times 10^{-1}\ O_2(aq) \\ &\rightarrow 3.4667 \times 10^{-3}\ HCO_3^- + 3.4701 \times 10^{-1}\ CrO_4^{2-} \\ &+ 1.1828\ Fe(OH)_3(aq) + 3.5167 \times 10^{-2}\ Mn^{2+} \\ &+ 9.9093 \times 10^{-3}\ NO_3^- + 1.8583 \times 10^{-1}\ Ni^{2+} \\ &+ 8.8004 \times 10^{-4}\ HPO_4^{2-} + 5.2008 \times 10^{-4}\ SO_4^{2-} \\ &+ 1.7325 \times 10^{-2}\ SiO_2(aq). \end{aligned} \quad (8)$$

The 304L stainless steel corrosion rate was assumed to be a constant 6.9×10^{-14} mol cm^{-2} s^{-1} [39] and not affected by changes in pH or water chemistry.

Table 2
Secondary phase reaction network for LAWABP1 glass

Reaction	log K (15°C)
$Al(OH)_3(am) \rightleftharpoons AlO_2^- + H^+ + H_2O$	−13.10
$Analcime \rightleftharpoons 0.96AlO_2^- + 0.96Na^+ + 2.04SiO_2(aq)$	−9.86
$Anatase + 2H_2O \rightleftharpoons Ti(OH)_4(aq)$	−6.64
$Baddeleyite + 2H_2O \rightleftharpoons Zr(OH)_4(aq)$	−9.29
$Goethite + H_2O \rightleftharpoons Fe(OH)_3(aq)$	−11.09
$Herschelite \rightleftharpoons 1.62Na^+(aq) + 0.50K^+(aq) + 2.26AlO_2^- + 4SiO_2(aq) + 0.14H^+ + 5.93H_2O$	−40.94
$La(OH)_3(am) + 3H^+ \rightleftharpoons 3H_2O + La^{3+}$	22.55
$Nontronite\text{-}K + 2H_2O \rightleftharpoons 0.330AlO_2^- + 2Fe(OH)_3(aq) + 0.330K^+ + 3.67SiO_2(aq)$	−43.70
$Nontronite\text{-}Mg + 2H_2O \rightleftharpoons 0.330AlO_2^- + 2Fe(OH)_3(aq) + 0.165Mg^{2+} + 3.67SiO_2(aq)$	−43.36
$Nontronite\text{-}Na + 2H_2O \rightleftharpoons 0.330AlO_2^- + 2Fe(OH)_3(aq) + 0.330Na^+ + 3.67SiO_2(aq)$	−43.33
$PuO_2 + H^+ + 0.25O_2(g) \rightleftharpoons PuO_2^+ + 0.5H_2O$	−5.18
$Sepiolite + 8H^+ \rightleftharpoons 4Mg^{2+} + 6SiO_2(aq) + 11H_2O$	31.29
$SiO_2(am) \rightleftharpoons SiO_2(aq)$	−2.85
$Weeksite + 2H^+ \rightleftharpoons 2K^+ + 2UO_2(OH)_2(aq) + 6SiO_2(aq) + 3H_2O$	−5.25
$Soddyite \rightleftharpoons 2UO_2(OH)_2(aq) + SiO_2(aq)$	−20.24
$Zn(OH)_2(am) + 2H^+ \rightleftharpoons 2H_2O + Zn^{2+}$	14.44

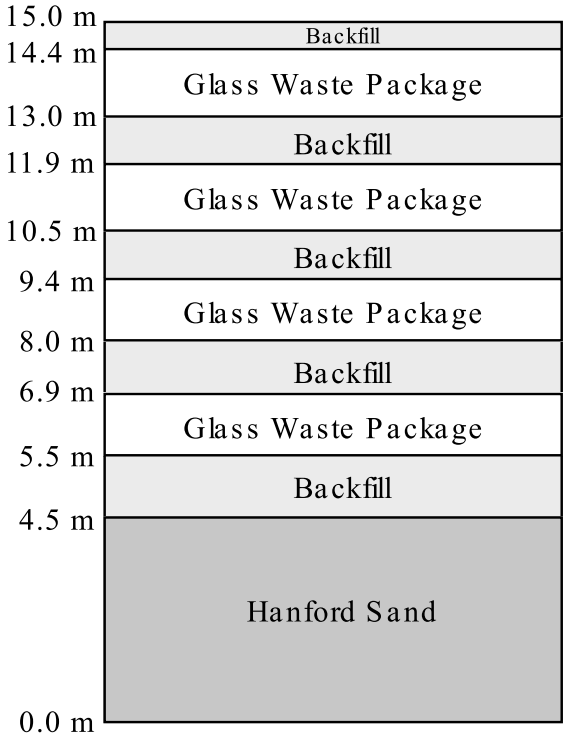

Fig. 10. Material zones for remote handled trench waste form release simulations.

Unsaturated hydraulic properties for the glass waste packages and backfill materials, used for calculating the water flow field, are listed in Table 3. Equilibrium with the atmosphere was assumed to be maintained throughout the spatial domain at all times. Model grids were 5 cm in vertical resolution. The time steps used in these calculations were calculated automatically by the code with a convergence criterion of 10^{-6}. This ensures that predicted values of aqueous species concentrations and mineral volumes are accurate between iterations for a given time step. If this cannot be achieved within a certain number of iterations, the time steps are automatically reduced. Numerous simulations were conducted to ensure that the grid spacing and convergence criteria chosen for the simulations were small enough to ensure accuracy, yet large enough to allow the simulations to finish in a reasonable amount of time. For comparison, the simulations were rerun with a grid spacing of 2.5 cm, and also with a convergence criterion of 5×10^{-7}. Results for these simulations were not significantly different than reported herein.

The flow simulations used the following boundary conditions: constant specified flux at the upper boundary and free drainage at the lower boundary. The reactive transport simulations used the following boundary conditions: specified aqueous species concentrations at the upper boundary and no diffusion across the lower boundary. The flux of Tc and the other radionuclides across the lower boundary is therefore limited to advection

$$f = c\rho_w v, \tag{9}$$

where c is the concentration (mol kg^{-1}); ρ_w the density of water (mol m^{-3}); v is the specific discharge (m s^{-1}).

The normalized flux to the vadose zone is calculated by summing fluxes at each grid node across the bottom boundary of the model, and normalizing the total flux according to the inventory in all the waste packages at the start of the simulation. The normalized flux across

Table 3
Best-estimate hydraulic parameter values for near-field materials[a]

Material	ρ_p (g cm^{-3})	ρ_b (g cm^{-3})	θ_s	θ_r	α (cm^{-1})	n	K_s (cm s^{-1})
Glass waste	2.68	2.63	0.02	0.00	0.2	3	0.01
Backfill	2.76	1.89	0.316	0.049	0.035	1.72	1.91×10^{-3}

[a] ρ_p – particle density; ρ_b – dry bulk density; θ_s – saturated water content; θ_r – residual water content; (α, n) – van Genutchen fitting parameters; K_s – saturated hydraulic conductivity.

the lower boundary, F, in units of ppm yr^{-1}, was calculated using

$$F = \frac{\sum_{i=1}^{N} f_i \Delta x_i \Delta y_i}{I}(3.1558 \times 10^7), \quad (10)$$

where f_i is the flux across the bottom of an individual grid block (μmol m^{-2} s^{-1}); $\Delta x_i \Delta y_i$ the cross-sectional area of an individual grid block (m^2); I is the inventory in the waste packages (mol m^{-3}), given by

$$I = V_{wp}(1 - \theta_T)V_G \rho_G \gamma_i, \quad (11)$$

where V_{wp} is the volume of the waste packages (m^3); θ_T the total porosity of the material representing the waste packages (0.02); V_G the fraction of each waste package that is glass (0.85); ρ_G the molar density of LAWABP1 glass (38 776 moles m^{-3}); γ_i is the mole fraction of radionuclide i in LAWABP1 glass (i.e., 6.59×10^{-1} μmol Tc mol^{-1} glass).The volume of the waste packages, V_{wp}, was 5.6 m^3. For 1- D simulations the cross-sectional area of the grid block was 1 m^2.

Two scenarios were considered: The base case was the RH trench with a recharge rate of 4.2 mm yr^{-1} and the second case was identical except for an assumed recharge rate of 0.9 mm yr^{-1}. A steady state, unsaturated flow field was calculated and used to provide water contents and water fluxes used in each of the transient reactive transport simulations.

5.2. Unsaturated flow field

Assuming steady-state flow with a constant recharge rate results in a constant water flux, equal to the recharge rate, throughout the entire depth of the profile. Water content, however, varies with depth in the profile. Water content is a dimensionless variable defined as the volume of water per volume of porous or fractured media. The unique relationship between water flux and water content for each material is defined by the hydraulic parameters listed in Table 3. Water contents are computed to be slightly lower inside the glass layers at a recharge rate of 0.9 mm yr^{-1} than at a recharge rate of 4.2 mm yr^{-1}, as shown in Fig. 11. These differences are insignificant, however, when compared with the two orders of magnitude difference in water content between the backfill and glass layers (Fig. 11). The large change in water content at the backfill/glass interfaces has a significant impact on the temporal evolution of the system, as will be discussed below.

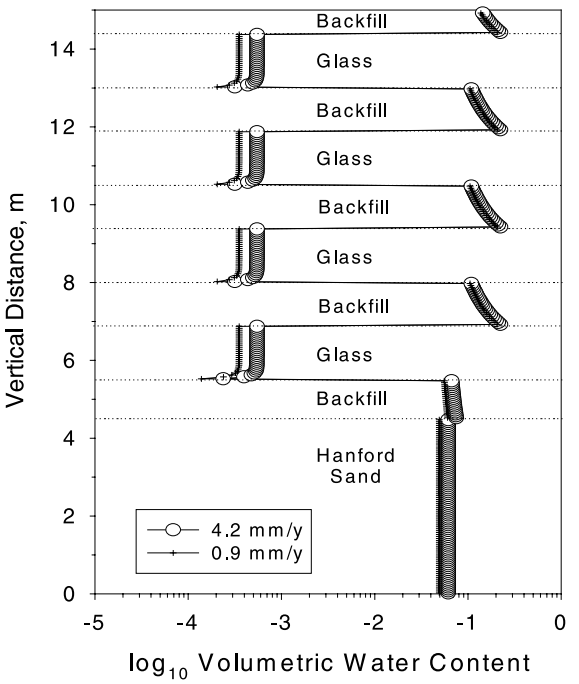

Fig. 11. Steady-state moisture content for the RH trench 1-D waste form release model at different recharge rates (horizontal dotted lines represent boundaries between material zones and material names shown along the right axis).

5.3. 1-D results

For the 1-D cases, it was conservatively assumed that glass dissolution was at the forward rate of reaction. In other words, buildup in the activities of species caused by glass dissolution, such as AlO_2^- and SiO_2(aq), was not considered to decrease the glass dissolution rate. In this case, only solution pH changes affected the calculated glass dissolution rate via Eq. (1). The calculated pH of pore water percolating through the system increases from a background value of 7 to a maximum value of 9.8 exiting the bottom of the facility, as shown in Fig. 12. The plot also shows an important impact of the two orders of magnitude difference in water content

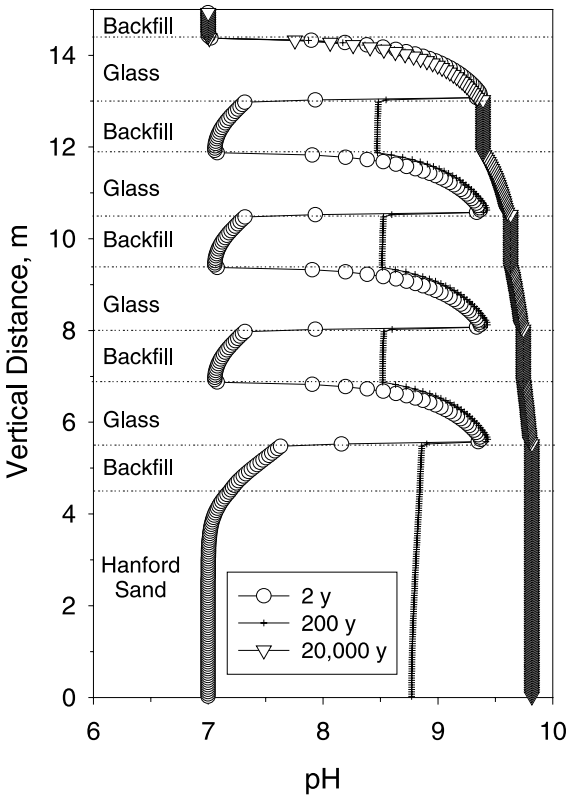

Fig. 12. pH for RH trench simulation with recharge rate of 4.2 mm yr^{-1} (horizontal dotted lines represent boundaries between material zones and material names are shown along right axis).

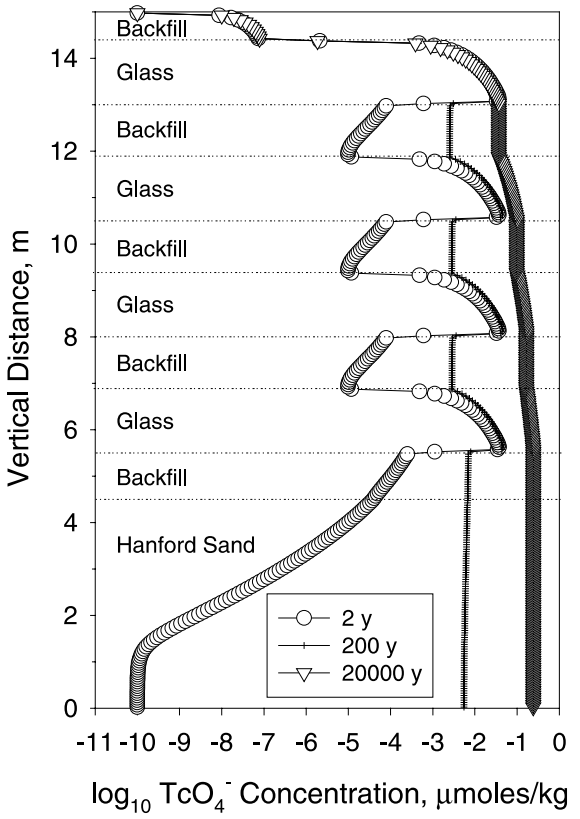

Fig. 13. Concentration of TcO_4^- for RH trench simulation with recharge rate of 4.2 mm yr^{-1} (horizontal dotted lines represent boundaries between material zones).

between the glass and backfill layers. Because of continuity boundary conditions at the interfaces, mass transport is required before changes to the initial conditions in the backfill layer can take place. The net result is that the backfill layers act like a storage reservoir, delaying and buffering increases in pH between the glass layers. In the first glass layer, an essentially steady-state pH profile is established in the first few years of the simulation. In contrast, deeper layers exhibit significant temporal changes resulting from the slow changes in the pore water pH in the backfill layers. Also, the cumulative effects of the reaction with preceding glass layers as water percolates through the disposal system are observed with pore water pH rising stepwise as a function of depth.

Similar results are observed for calculated TcO_4^- concentrations as shown in Fig. 13. At early times, the TcO_4^- concentrations increase sharply in the glass layers. Glass dissolution, and low water contents in the glass layers, coupled with a low water flux rate, causes TcO_4^- concentrations to increase rapidly in the glass layers. In contrast, mass transport from the glass layers is required to buildup Tc concentrations in the backfill layers. Therefore, concentrations in the backfill layers increase slowly as products of glass dissolution diffuse from the glass layers into the backfill layers, where dilution also occurs because of the much higher water content in the backfill layers compared with the glass layers.

The maximum flux of Tc to the vadose zone for the RH trench base case simulation is 8.4 ppm yr^{-1} at 20 000 yr (Fig. 14). The Tc flux to the vadose zone is proportional to the TcO_4^- concentration at the lower boundary and the water flux rate (see Eq. (7)). The maximum flux of Tc to the vadose zone for the case where the recharge was lowered to 0.9 mm yr^{-1} is only 0.98 ppm yr^{-1} at 20 000 yr (Fig. 14). This is 8.5 times lower than the maximum flux predicted by the RH trench simulation with a 4.2 mm yr^{-1} recharge rate. Concentrations of TcO_4^- were higher in the glass layers at the lower recharge rate as were solution pH and glass dissolution rates. Higher glass dissolution rates are expected at lower rates of recharge because the decrease in flow rate means less influx of low pH and low ionic strength fluid into the system, driving the pH higher in the glass layers. However, TcO_4^- concentrations at the lower boundary are lower than seen in the base case simulation at 4.2 mm yr^{-1} recharge. Although glass release rates are

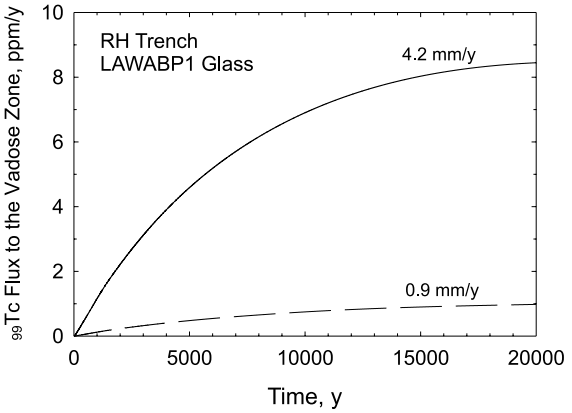

Fig. 14. Technetium flux across bottom boundary of model.

higher at 0.9 mm yr^{-1}, lower water contents in the glass layers for this case result in even lower rates of diffusion from the glass layers into the backfill layers. This, coupled with a lower water flux, results in a lower overall flux to the vadose zone.

5.4. 2-D results

Calculations in 2-D were conducted using the same base case recharge rate of 4.2 mm yr^{-1} and other assumptions used for the 1-D calculations, with the exception that the full rate law for glass dissolution was used including the mixed Al–Si activity product for the chemical affinity. Consequently, glass reactions rates are affected by pH and the activities of AlO_2^- and SiO_2(aq). Fig. 15 shows the calculated saturation index (Q/K_g) for the glass at 20 000 yr. The outlines of the waste package regions can be clearly discerned in this plot by the dark green areas with closely spaced contour bands. The calculations show that the pore water is significantly undersaturated with the respect to the mixed Al–Si activity product (Eq. (3)) with $\log_{10} Q/K_g < -2$.

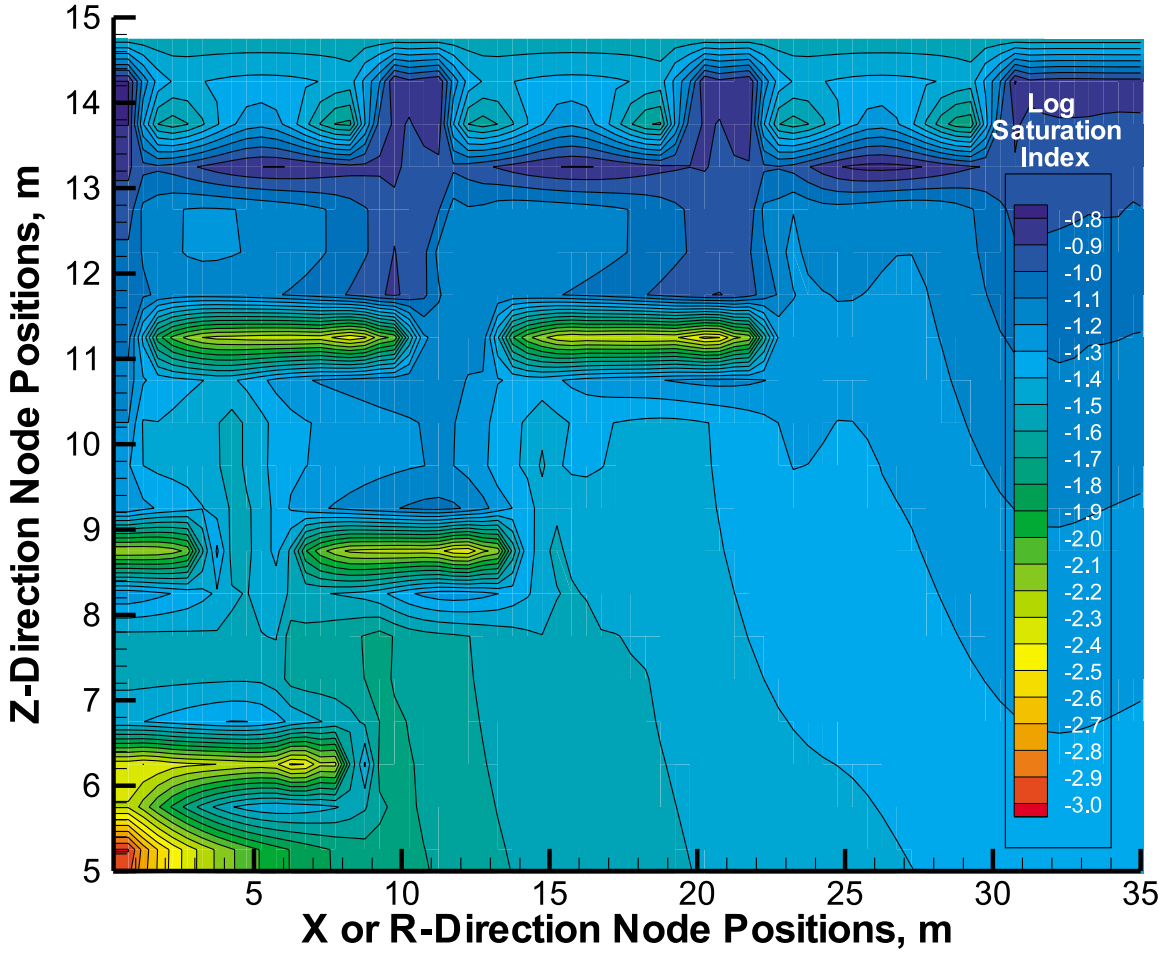

Fig. 15. Log_{10} saturation index for LAWABP1 glass based on mixed Al–Si pseudoequilibrium constant.

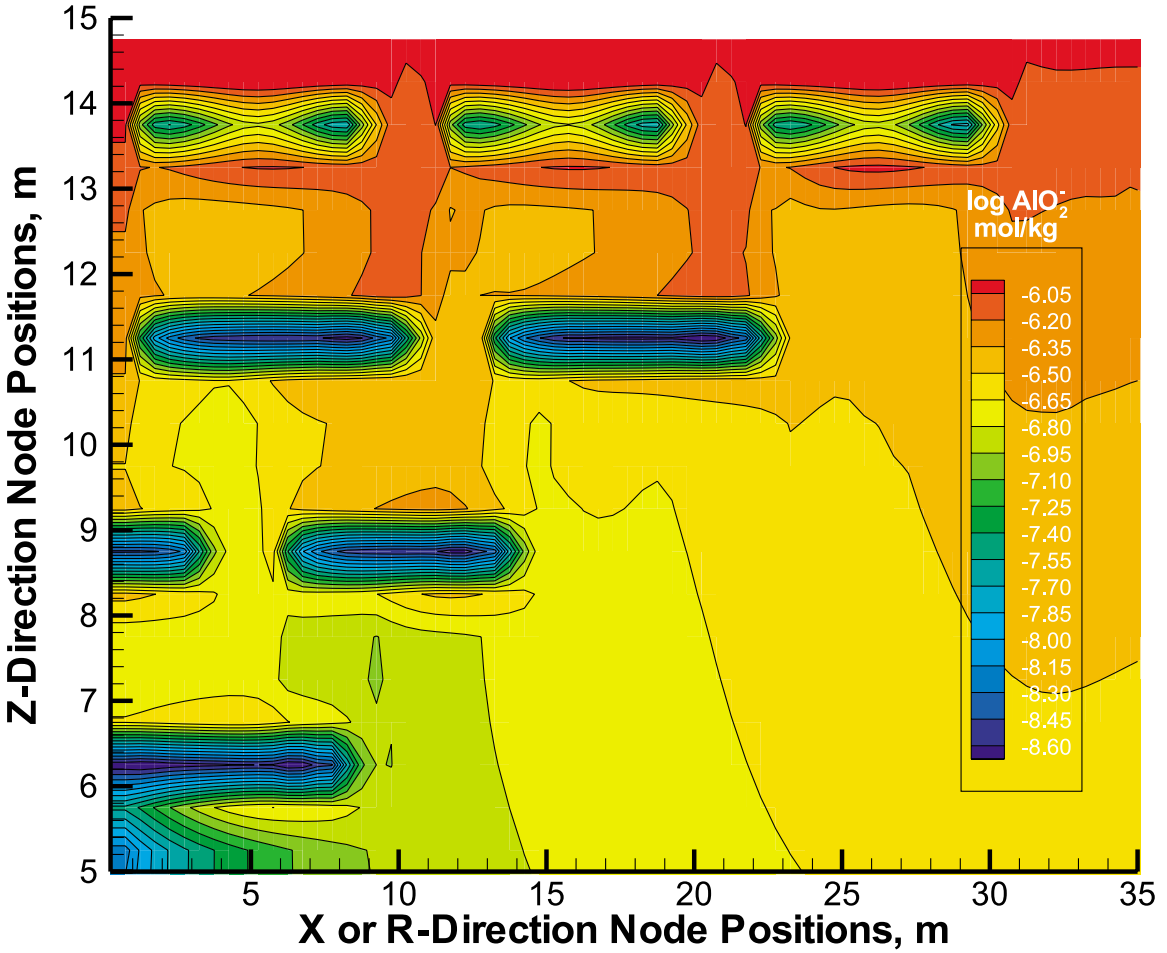

Fig. 16. Calculated aluminate concentration distribution in LAW disposal system at 20 000 yr.

Consequently, the glass is predicted to be dissolving at near the forward rate of reaction in these simulations.

This result is quite surprising because the same simulations show that the pore water in contact with the glass is at or near saturation with respect to SiO_2(am). Clearly, a silicate glass would not dissolve at near forward reaction in a silica-saturated solution. The discrepancy can be resolved by examining the calculated concentration distribution of AlO_2^-, as shown in Fig. 16. The data show very low AlO_2^- concentrations in the waste packages, approaching 10^{-9} M near the bottom of the trench. The low AlO_2^- concentrations result because Al is being consumed from precipitation of several aluminosilicate alteration phases in the waste package region, including herschelite and Na-nontronite. Although there is sufficient Si available from glass dissolution to maintain SiO_2(aq) concentrations to near saturation with respect to amorphous silica, the Al concentrations drop to such low values that this term dominates the mixed Al–Si activity product (Eq. (3)), resulting in a small effective saturation index for the glass. The net result is that LAWABP1 glass is predicted to be dissolving at the forward rate of reaction in a silica-saturated solution.

6. Discussion

6.1. Kinetic rate law for glass dissolution

Because of the experimental observation that Al can have a significant impact on the dissolution kinetics of waste glasses, several investigators have advocated the inclusion of Al in Grambow's [15] original kinetic rate law for glass dissolution in an inhibitor term, $\prod a_j^{\eta_j}$ [23], or as part of mixed Al–Si pseudoequilibrium constant to be used in the chemical affinity $(1 - Q/K_g)$ portion of the rate law [24,27]. Either approach can provide improved fits for some data sets, similar to our observations for LAWABP1 glass as documented in Fig. 5. However,

adoption of either approach in PA calculations can lead to cases where silicate glasses are predicted to dissolve at forward reaction rate in silica-saturated solutions, clearly an impossible result. This occurs because the disposal system can evolve chemically in reactive transport simulations to conditions very different from the experiments that were used to derive the rate law parameters. As an inhibitor, the η_{Al} term in the activity product must be negative. As $a[AlO_2^-] \rightarrow 0$, the inhibitor term becomes very large and so the calculated glass dissolution rates become large. Similarly for the chemical affinity term, as $a[AlO_2^-] \rightarrow 0$, $Q/K_g \rightarrow 0$ and the glass is predicted to dissolve at the forward rate of reaction. Clearly, neither the inhibitor approach nor chemical affinity approach with a mixed Al–Si activity product works well in a kinetic rate law intended for general use in PA simulations. It is apparent that a new kinetic rate law for glass dissolution is needed that can account for the observed effects of inhibitor species, such as aluminate, and yet remain mathematically stable for calculations in chemically evolving systems where the activities of inhibitor species (such as AlO_2^-) can drop to very low values.

6.2. Disposal system performance

The results from the 1-D STORM simulations of the near field were combined with far field transport, groundwater flow and transport to a well 100 m downgradient, and dosimetry information for several representative population groups to provide estimated impacts for the proposed ILAW disposal action. Details regarding these calculations and additional results can be found in reference [7]. The ≈ 8 ppm yr^{-1} release rate at 20,000 yr from the near field at 4.2 mm yr^{-1} recharge rate translates into a beta/photon dose from ^{99}Tc and ^{129}I of approximately 0.2 mrem yr^{-1}, as shown in Fig. 17. This is a factor of 20 less than the 4 mrem yr^{-1}

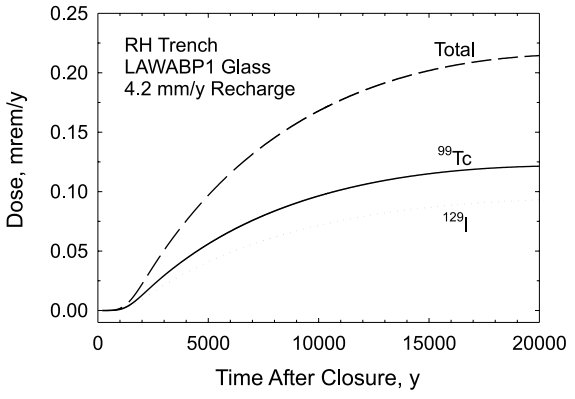

Fig. 17. Time dependence for RH trench beta/photon drinking water dose to 20 000 yr.

performance objective for protecting groundwater resources at the Hanford Site. Considering that the 1-D simulations were performed such that the glass was forced to dissolve at the forward rate of reaction, an even larger margin of safety would be calculated for the case where the chemical affinity term in Eq. (1) was allowed to reduce the glass reaction rate in the disposal facility.

Of course, the preceding analysis is only strictly valid for the case where LAWABP1 glass was manufactured and disposed in the ILAW facility. However, final selection of ILAW glass compositions have not been made and because of waste stream variability and processing considerations, it is a virtual certainty that the final ILAW glass forms will differ in composition from LAWABP1 glass. If ILAW glasses were made that had higher Na_2O loading and/or had significantly faster rates of alkali ion exchange, higher solution pH in the disposal facility would result and the available margin of safety could be significantly reduced.

To assess the likelihood that ILAW glass waste forms can be produced that have long-term durability characteristics approximating that of LAWABP1 glass, the relative performance of a wide range of ILAW glass compositions were compared using the VHT [21]. Briefly, in the VHT, monolithic samples are exposed to saturated water vapor at elevated temperatures (typically 100–300°C) in a sealed vessel. This environment greatly accelerates the progression of glass corrosion by water and can result in the formation of alteration phases. A matrix of 56 glass compositions was subjected to VHTs at 200°C for sufficiently long periods of time to obtain a statistically meaningful measure of the glass corrosion rate. The glasses varied the concentrations of SiO_2, Al_2O_3, B_2O_3, Fe_2O_3, TiO_2, ZnO, ZrO_2, MgO, and Na_2O across a wide composition range that covers, with high probability, the expected processing composition range for candidate ILAW glasses. For details on the specific glass compositions involved, please see [21].

The VHT corrosion rate data of Vienna et al. [21] have been plotted in the form of a cumulative distribution function, shown in the Fig. 18. The measured 200°C VHT corrosion rate for LAWABP1 glass is 4.8 g m^{-2} d^{-1} and the corresponding data point is highlighted in Fig. 18. LAWABP1 glass is very near the midpoint of the distribution (half of the data set have higher rate and half lower) of 5.1 g m^{-2} d^{-1}. A full 80% of the tested glasses have 200°C VHT corrosion rates less than 30 g m^{-2} d^{-1}, which is about 7 times faster than the VHT rate for LAWABP1 glass. However, a glass reacting 7 times faster than LAWABP1 would still fall well within the margin of safety available to meet groundwater pathway performance objectives. Based on these results, it appears to be a virtual certainty that glasses can be formulated and manufactured that will meet performance objectives for disposal of low- activity tank wastes.

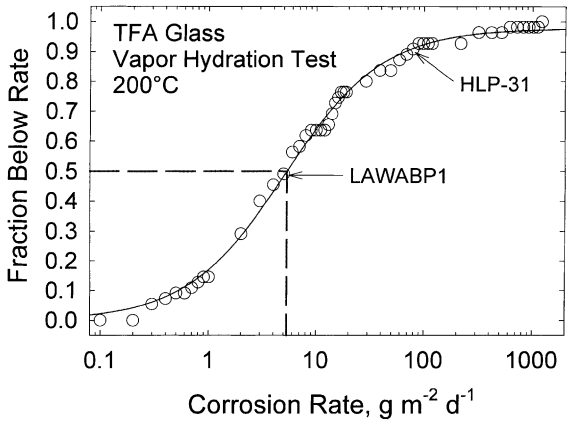

Fig. 18. Cumulative distribution plot of 200°C VHT corrosion rates for HLP series of ILAW Glasses. Approximately 80% of the test glasses have VHT corrosion rates at 200°C less than 30 g m^{-2} d^{-1}. The data were fit to a three-parameter logistic function of the form $y = a/[1 + (x/x_0))^b]$.

7. Conclusion

Reactive chemical transport calculations were performed to analyze the long-term performance of a LAW glass in a proposed disposal facility at the Hanford Site. Parameterization of the reactive transport model was performed through a combination of laboratory experimentation, extraction of relevant data from the literature (principally thermodynamic data), and through parameter estimation. Even with conservative assumptions, calculated release rates from the facility were lower than the performance objectives by a factor of 20. Vapor hydration experiments with a wide variety of LAW glass formulations suggest a large composition space is available from which glasses can be made that are as or more durable than LAWABP1 glass. STORM simulations using a mixed Al–Si ion activity product predicted glass dissolution rates at near the forward reaction rate in solutions that were saturated with respect to amorphous silica, an impossible result. Thus, a mixed Al–Si ion activity product should not generally be used for modeling glass dissolution behavior in performance assessments.

Acknowledgements

The authors would like to credit Elsa Rodriguez for her outstanding work in conducting the SPFT experiments discussed in this paper, and Chris Brown and Matt O'Hara for their skill in analyzing the thousands of solution samples we generated. We also thank Eugene Freeman and Scott Finfrock for their work in calculating the contaminant transport through the vadose zone and the estimation of human dose. The authors would also like to thank Neil Brown, Phil LaMont, and Carol Babel at the Office of River Protection for their strong support of our research related to low-activity tank waste disposal at Hanford. This work was funded by the US Department of Energy under Contract DE-AC06-76RLO 1830.

References

[1] B.P. McGrail, W.L. Ebert, D.H. Bacon et al., A strategy to conduct an analysis of the long-term performance of low-activity waste glass in a shallow subsurface disposal system at Hanford, PNNL-11834, Pacific Northwest National Laboratory, Richland, WA.

[2] J.S. Small, P.N. Humphreys, T.L. Johnstone et al., Mater. Res. Soc. Symp. Proc. 608 (2000) 129.

[3] SKB, Deep Repository for Spent Nuclear Fuel. SR97 – Post closure safety, Main Report Summary, TR-99-06, Swedish Nuclear Fuel and Waste Management, Stockholm, Sweden.

[4] JNC, H12: Project to Establish the Scientific and Technical Basis for HLW Disposal in Japan, JNC TN1410 2000-001, Japan Nuclear Cycle Development Institute, Tokai-mura, Japan.

[5] Department of Energy, Viability assessment of a repository at Yucca mountain, DOE/RW-0508, US Department of Energy, Washington, DC.

[6] D.R. Anderson, G. Basabilvazo, J.C. Helton et al., Performance assessment in support of the 1996 compliance certification application for the waste isolation pilot plant, SAND98-1756J, Sandia National Laboratories, Albuquerque, NM.

[7] F.M. Mann, R.J. Puigh II, S.H. Finfrock et al., Hanford immobilized low-activity tank waste performance assessment: 2001 Version, DOE/ORP-2000-24 Rev. 0, US Department of Energy, Richland, WA.

[8] CRWMS M & O, Total system performance assessment – viability assessment (TSPA-VA) analyses technical basis document, Chapter 6, Waste Form Degradation, Radionuclide Mobilization and Transport Through the Engineered Barrier System. B00000000-01717- 4301-00006, Rev. 01., MOL.19981008.0006., Civilian Radioactive Waste Management System, Las Vegas, NV.

[9] R.J. Puigh II, Disposal facility data for the Hanford immobilized low-activity tank waste, HNF-4950 Rev. 1, Fluor Federal Services, Richland, WA.

[10] C.T. Kincaid, J.W. Shade, G.A. Whyatt et al., Performance assessment of grouted double-shell tank waste disposal at Hanford, WHC-SD-WM-EE-004 Rev. 1, Westinghouse Hanford Company, Richland, WA.

[11] F.M. Mann, R.J. Puigh II, P.D. Rittmann et al., Hanford immobilized low-activity tank waste performance assessment, DOE/RL- 97-69 Rev. 0, US Department of Energy, Richland, WA.

[12] D.H. Bacon, M.D. White, B.P. McGrail, Subsurface transport over reactive multiphases (STORM): a general, coupled nonisothermal multiphase flow, reactive transport, and porous medium alteration simulator, Version 2, User's

Guide, PNNL-13108, Pacific Northwest National Laboratory, Richland, WA.
[13] P.S. Huyakon, S. Panday, VAM3DF – Variably saturated analysis model in three dimensions for the data fusion system: documentation and user's guide, Version 2.0, HydroGeologic, Herndon, VA.
[14] P. Aagaard, H.C. Helgeson, Am. J. Sci. 282 (1982) 237.
[15] B.E. Grambow, Mater. Res. Soc. Symp. Proc. 44 (1985) 15.
[16] D.M. Strachan, W.L. Bourcier, B.P. McGrail, Radioactive Waste Management Environ. Restoration 19 (1994) 129.
[17] S. Gin, C. Jégou, E. Vernaz, Appl. Geochem. 15 (2000) 1505.
[18] C. Jégou, S. Gin, F. Larché, J. Nucl. Mater. 280 (2000) 216.
[19] B.P. McGrail, P.F. Martin, C.W. Lindenmeier et al., in: L.G. Mallinson (Ed.), Ageing Studies and Lifetime Extension of Materials, Kluwer Academic/Plenum, New York, 2001, p. 313.
[20] B.P. McGrail, J.P. Icenhower, P.F. Martin,et al., Waste form release data package for the 2001 immobilized low-activity waste performance assessment, PNNL-13043 Rev. 2, Pacific Northwest National Laboratory, Richland, WA.
[21] J.D. Vienna, A. Jiricka, B.P. McGrail et al., Hanford immobilized LAW product acceptance testing: initial data package, PNNL-13101, Pacific Northwest National Laboratory, Richland, WA.
[22] E.H. Oelkers, J. Schott, J.-L. Devidal, Geochim. Cosmochim. Acta 58 (9) (1994) 2011.
[23] T.J. Advocat, J.L. Chouchan, J.L. Crovisier et al., Mater. Res. Soc. Symp. Proc. 506 (1998) 63.
[24] S. Gin, Mater. Res. Soc. Symp. Proc. 412 (1996) 189.
[25] A.C. Lasaga, in: A.F. White, S.L. Brantley (Eds.), Chemical Weathering Rates of Silicate Minerals, Reviews in Mineralogy, Mineralogical Society of America, Washington, DC, 1995.
[26] B.P. McGrail, W.L. Ebert, A.J. Bakel, et al., J. Nucl. Mater. 249 (1997) 175.
[27] P.K. Abraitis, B.P. McGrail, D.P. Trivedi, et al., J. Nucl. Mater. 280 (2) (2000) 206.
[28] W.L. Bourcier, S.A. Carroll, B.L. Phillips, Mater. Res. Soc. Symp. Proc. 333 (1994) 507.
[29] B.P. McGrail, P.F. Martin, C.W. Lindenmeier, Corrosion testing of low-activity waste glasses: Fiscal Year 1998 Summary Report, PNNL-12014, Pacific Northwest National Laboratory, Richland, WA.
[30] B.P. McGrail, J.P. Icenhower, D.K. Shuh et al., J. Non-Cryst. Solids (2001) in press.
[31] Y. Chen, B.P. McGrail, D.W. Engel, Mater. Res. Soc. Symp. Proc. 465 (1997) 1051.
[32] ASTM, Standard Test Methods for Determining Chemical Durability of Nuclear Waste Glasses: the Product Consistency Test (PCT), American Society for Testing and Materials, Philadelphia, PA.
[33] T.J. Wolery, S.A. Daveler, EQ6, A computer program for reaction path modeling of aqueous geochemical systems: theoretical manual, user's guide and related documentation, UCRL-MA-110662 PT IV, Lawrence Livermore Laboratory, Livermore, CA.
[34] S.A. Daveler, T.J. Wolery, EQPT, A data file preprocessor for the EQ3/6 software package: user's guide and related documentation (Version 7.0), UCRL-MA-110662 PT II, Lawrence Livermore National Laboratory, Livermore, CA.
[35] S.V. Mattigod, B.P. McGrail, Microporous Mesoporous Mater. 27 (1999) 41.
[36] S.V. Mattigod, J.A. Kittrick, Soil Sci. Soc. Am. J. 44 (1980) 149.
[37] R.D. Peters, S.C. Slate, Nucl. Eng. Design 67 (1981) 425.
[38] R.K. Farnsworth, M.K.W. Chan, S.C. Slate, Mater. Res. Soc. Symp. Proc. 44 (1985) 831.
[39] P.L. Cloke, D.M. Jolley, D.H. Lester, Waste package development design analysis, BBA000000-01717-0200-0050 Rev. 00, CRWMS M & O, Las Vegas, NV.